Rev. Adv. Mater. Sci. 43 (2015) 67-76

IMPEDANCE SPECTROSCOPY STUDY OF ZrO_2-HfO_2-Y_2O_3 SOLID ELECTROLYTES

N.N. Novik[1,2], O.V. Glumov[1], S.N.Golubev[3], V.G.Konakov[1,2] and I.Yu. Archakov[2,4]

[1]Institute of Chemistry, St. Petersburg State University, Universitetskiy pr. 26, Petrodvorets, St. Petersburg, 198504, Russia
[2]Research Laboratory for Mechanics of New Nanomaterials,
Peter the Great St. Petersburg Polytechnic University, Polytechnicheskaya 29, St. Petersburg, 195251, Russia
[3]Scientific and Technical Center “Glass and Ceramics”8, 20 lit. A, 9 linia V.O., St. Petersburg, 199004, Russia
[4]Institute of Problems of Mechanical Engineering, Russian Academy of Science, Bolshoy pr.61, V.O., St. Petersburg, 199178, Russia

Received: October 05, 2015

Abstract. Solid solutions of ternary ZrO_2-HfO_2-Y_2O_3 system are the perspective materials to replace conventional yttria-stabilized Zirconia materials in electrochemical applications due to higher thermal stability and lower input of electronic conductivity at low oxygen partial pressures. Samples with 8 mol.% Y_2O_3 and HfO_2 content from 5 to 20 mol.% were manufactured from nanosized precursors synthesized by sol-gel reverse co-precipitation technique. The structure of the samples was studied, particle size and phase composition were the points of essential interest. Impedance spectroscopy data provide the opportunity to separate grain and grain boundary inputs into the integral ceramics conductivity, these data were used to consider the grain boundary phase features. The conductivity dependence on sample chemical composition was determined.

1. INTRODUCTION

Ceramics based on yttria-stabilized zirconia (YSZ) is widely used in solid oxide fuel cells [1,2] and electrochemical sensors [3] due to its high thermal and chemical stability coupled with electrochemical characteristics suitable for these applications. The use of pure zirconia here is impossible due to low electroconductivity and insufficient mechanical properties at high temperatures because of the negative effect of monoclinic↔ tetragonal (m↔t) transition with the transition temperature of 1200 °C (data for extra pure zirconia). The addition of yttrium oxide (conventionally, 8 mol.%) gives an opportunity to stabilize cubic fluorite-like solid solution possessing stable mechanical properties at elevated temperatures. In addition, this solid solution is characterized by a high number of oxygen vacancies providing high values of ionic conductivity.

The investigation of the correlations of YSZ-based materials internal structure with their exploitation and electrical characteristics is one of the important points of modern studies in this field. The study of submicron- and nanoceramics, i.e. the ceramics with the electrolyte grain size lying in submicron or nano range, along with ceramics manufactured from submicron or nanosized precursors is of current interest since such materials are considered as very perspective [4]. This is due to the fact that variation of particle size and changes in material treatment procedure provide the possibility to affect the ceramics conductivity. However, there is a number of problems with zirconia-based ceramics applications at temperatures much higher than 1200 °C, as well

Corresponding author: N.N. Novik, e-mail: nikn.novik@gmail.com

as at low oxygen partial pressures. According to [5], the latter is due to the fact that electronic conductivity typical for such objects at p_{O_2} <10^{-13} Pa [5]. In addition, the transition layer containing the components originated from bulk ceramics [6] can be formed on the solid electrolyte surface. In turn, this phenomenon can add some undefined diffusion potential to the electromotive force (EMF) of the galvanic cell used in electrochemical sensor. Above problems limit the application of zirconia-based materials in high-temperature processes typical for metallurgy, glass manufacturing, etc.

One of the possible approaches to overcome these problems can be the use of hafnium dioxide instead of zirconia. It was shown that electrolytes based on yttrium-stabilized HfO_2 possess higher chemical stability and are less sensitive to temperature changes than YSZ-based materials, see, e.g. [7]. In addition, the lower electronic conductivity at 1200 °C is reported for HfO_2-based electrolytes [7], while the ionic conductivities of both materials are comparable. However, the high cost of hafnium dioxide prevents its wide use. The alternative approach coupling the advantages of both materials is the application of ternary ZrO_2-HfO_2-Y_2O_3 solid solution. It should be mentioned that the information on the peculiarities of the conductivity structure in the ternary solid solutions is insufficient. On the other hand, there are some data demonstrating that the addition of the third component can significantly change the inputs of different conductivity components. The authors of [8] reported that stabilization of the cubic zirconia-based solid solution by both yttrium and magnesium oxides results in the complete elimination of the grain boundary input. Electrochemical properties of (92-*x*)ZrO_2-*x*HfO_2-8Y_2O_3 (5<*x*<15 mol.%) ceramics were studied in [9]. However, the study was performed at one current frequency only, this approach does not provide the information on the correlation between the ceramics structure and its electrochemical properties; moreover, it can be a source of some misinterpretation. Impedance spectroscopy is considered as one of the most effective approaches to study such electrochemical processes. This technique is based on the study of the system response on the application of the alternating current with different frequencies that makes possible to separate the inputs of phase transitions (including grain and grain boundaries) and some other phenomena in the integral conductivity of polycrystalline ceramics [10]. In particular, the input attributed to ceramic components can be identified by impedance spectroscopy. So, this approach is very effective for ternary systems since it clarifies the conductivity variations due to the third component introduction. On the other hand, one should mention that impedance spectrometry data treatment requires the detailed study of the ceramics structure to understand the solid solution properties and electrochemical characteristics because some different processes can produce similar spectral response.

The aim of the present work was the study of the electrochemical properties of ZrO_2-HfO_2-Y_2O_3 composite with hafnium oxide content up to 15 mol.% by impedance spectroscopy. The samples were manufactured from nanosized precursor powders, the control of the particle size in these precursors was a point of essential interest. A set of various approaches giving the information on the ceramics structure was used to interpret the impedance spectroscopy data.

2. EXPERIMENT

2.1. Synthesis of the precursor powders

Sol-gel reverse co-precipitation was used to produce precursor powders of 87 mol.% ZrO_2 – 8 mol.% Y_2O_3-5 mol.% HfO_2 (here and after – Sample 1), 82 mol.% ZrO_2 – 8 mol.% Y_2O_3-10 mol.% HfO_2 (Sample 2), and 77 mol.% ZrO_2 – 8 mol.% Y_2O_3-15 mol.% HfO_2 (Sample 3), the following initial reagents were used: $ZrO(NO_3)_2$•$5H_2O$ (Acros Organics), $Y(NO_3)_3$•$6H_2O$ (Acros Organics), $HfOCl_2$•$8H_2O$, and aqueous ammonia. 0.1 M salt solution was prepared, this solution was added into 1 M NH_4OH solution at 2 mL/min rate at permanent stirring by multiblade mechanical stirrer. The gel synthesis was performed in the ice bath at 0-2 °C at constant pH of 9-10. The produced gel was separated from the solution and washed up to neutral reaction of the washing water, the completeness of Cl^- elimination was also checked by silver nitrate. The washed gel was dried under the elevated pressure: some part of the gel was rubbed up between two chemically inert surfaces; the surfaces were loaded by a weight of 1 kg and placed into a drying cabinet. The drying was carried out at 110 °C for 10 minutes. A part of the obtained powder was annealed at 600 °C for two hours and then milled in Pulverisette 6 planetary mill (420 rpm, 20 reverse cycles for 5 minutes each cycle). Note that such powder will be called “treated powder” below. The treated powder was pressed at 5 ton per cm^2 for 5 minutes; as a result, 7.8 mm in diameter and 2.4 mm in height tablets were produced, they were used to study electrochemical impedance.

2.2. Precursor powders study

Temperatures and types (exo or endo) of the phase transitions in the precursor powders were studied by Differential Scanning Calorimetry using «Netzsch STA 449 F3 Jupiter», the heating rate was 20 °C/min. Scientific research was performed at the Center for Thermogravimetric and Calorimetric Research of Research park of St. Petersburg State University.

Particle size distribution analysis (Horiba LA950) was used to control the particle size in the precursor powders. Phase composition was determined by XRD (SHIMADZU XRD-600, Cu-K_α irradiation at λ = 1.54 Å, room temperature. XRD data (the shape of the most intensive reflex) were also used to estimate crystallite size according to Sherrer's formula:

$$d_{xrd} = K\frac{57.3\alpha}{\Delta\cos\theta}, \quad (1)$$

where d_{xrd} is the size of the coherent scattering region (the average crystallite size), θ - Bragg's angle for diffraction scattering, K – Sherrer's constant depending on the crystallite shape (K is equal to 1 here), λ - the irradiation wavelengths (1.54 Å), and Δ - the width of the reflex on its half height, degrees.

The microstructure of the ceramics was studied by SEM (Hitachi S-3400N microscope with EDX analysis unit AzTec Energy 350, accelerating voltage was 20 kV here). EDX data provides the control of the ceramics sample composition. SEM and EDX study were performed at the Center for Geo-Environmental Research and Modeling (GEOMODEL) of Research park of St. Petersburg State University.

The surface area of the precursor powders was estimated by BET method from the adsorption-desorption data obtained by ASAP 2020 MP, nitrogen was used as an adsorbed gas. Note that all samples were dried at 200 °C in vacuum before adsorption-desorption tests. The average particle size in the ceramics was calculated from the data on the surface area as:

$$d_{BET} = \frac{6\cdot10^{-4}}{\rho S_{BET}}, \quad (2)$$

where d_{BET} is the average particle size, ρ – the theoretical density of the material with a given chemical composition, and S_{BET} – relative surface area according to the adsorption-desorption data. BET study was performed at the Center for Innovative Technologies of Composite Nanomaterials of Research park of St. Petersburg State University.

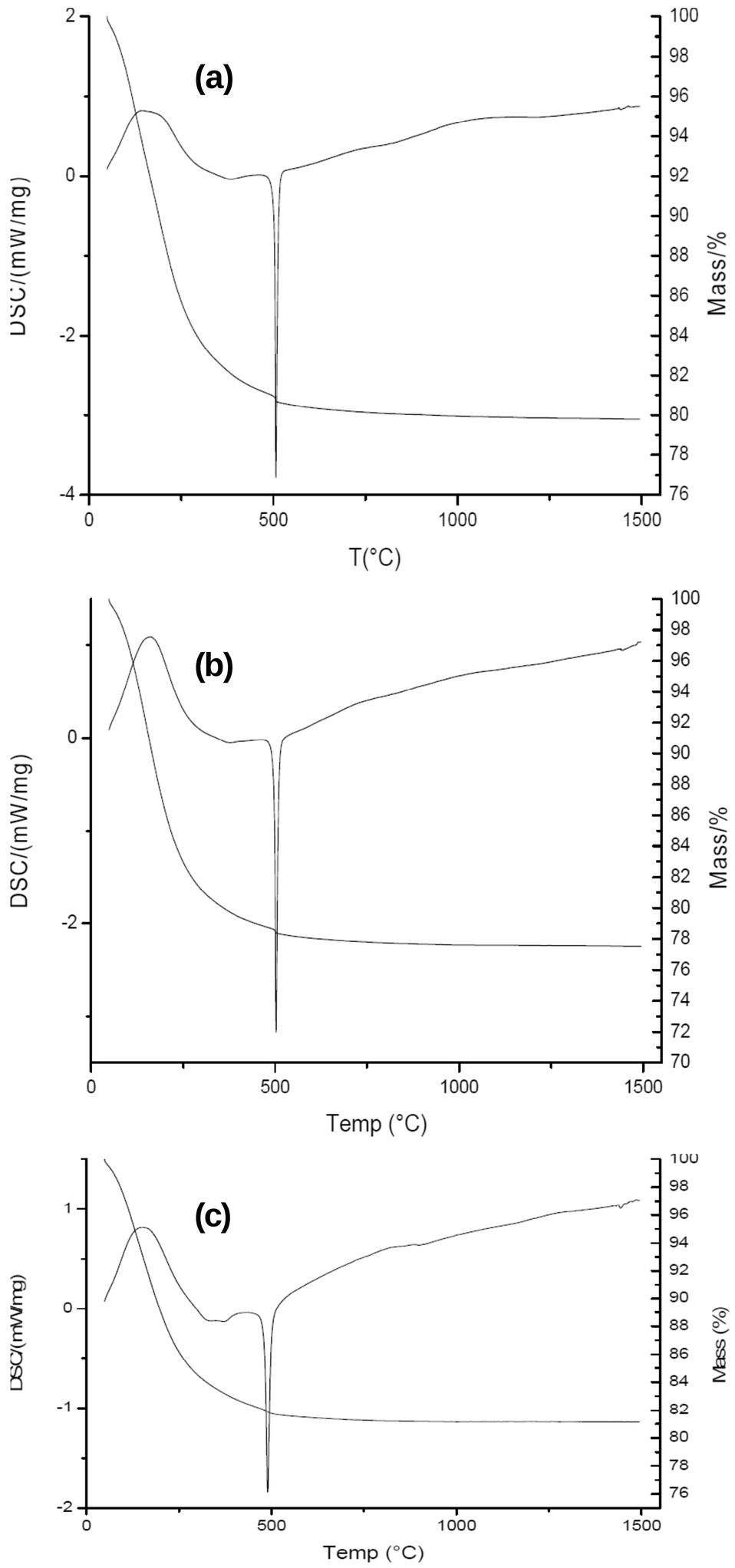

Fig. 1. DSC and TG curves for Sample 1 (a), 2 (b), and 3 (c).

2.3. Study of the electrochemical properties

Electrochemical impedance approach was used to investigate the electrochemical properties of the manufactured samples. Platinum paste was placed at the surface of ceramic tablets to provide proper contact with electrodes; samples with the paste were subjected to thermal treatment at 1100 °C for two hours. Electrochemical impedance was measured in the temperature range from 250 to 650 °C; experiments were performed in the quartz cell with Pt contacts and wires using Autolab PGSTAT 302N Potentiosytat/Galvanostat.

Table 1. Characteristic temperatures of the effects observed on the DSC curves.

Sample	1	2	3	Effect type
T, °C	129	153	150	endo
	-	-	365	exo
	506	502	488	exo

3. RESULTS AND DISCUSSION

3.1. Phase transition temperatures

Fig. 1 demonstrates DSC and thermogravimetry curves obtained for the studied samples, the determined temperature of endo- and exo- effects is listed in Table 1. Let us discuss these data in more detail. Some wide endothermic peak is observed for all samples in the temperature range from 100 to 300 °C. According to the thermogravimetry data, this effect is characterized by the significant loss in the sample weight. Following [11], we consider it to be due to the loss of structure- and chemically bound water, at that, $Zr(OH)_4$ decomposes to $ZrO(OH)_2$. The following zirconium hydroxide decomposition resulting in the amorphous zirconia formation takes place at higher temperatures.

Exothermic effect observed for all samples at temperatures ~ 500 °C is attributed as being due to crystallization process, this fact is supported by XRD data (see below), the weight loss here is negligible. As seen from Table 1, the temperature of this effect is quite similar for all samples, thus, the crystallization temperature of the amorphous precursor powder can be considered as being independent of the sample composition. Sample 3 demonstrated an additional exothermic peak at 365 °C, similar effect was reported in [12] for ZrO_2-CaO powder that was also synthesized by sol-gel synthesis. This effect can be explained as some onset of slow crystallization, one can expect the traces of this effect for Samples 1 and 2 also.

3.2. Precursor composition

Sol-gel synthesis in its reverse coprecipitation form manifests itself as an approach providing the final ceramics composition close to the initials reagents one. However, the presence of isotropic Hf ion admixture into the zirconyl nitrate $ZrO(NO_3)_2 \cdot 5H_2O$ (according to Acros data, it can be up to 4 wt.%) makes possible some deviations from the required sample composition. Table 2 presents the composition of the synthesized ceramic samples, note that the element content here is recalculated from the direct experimental data regarding for their oxide form. As seen from the table, the final content of hafnium dioxide in the samples studied is higher than that expected from the initial stoichiometric composition at synthesis. However, the prediction of the final composition of the ceramics was not possible since the input of hafnium admixture in zirconyl nitrate was unknown; it varies from batch to batch.

3.3. Precursor powders structure

The particle size in the precursor powders is a point of essential interest since it was shown (see, e.g. [13]) that ceramics properties, including electrochemical, depend both on the grain size in the final ceramics and on the particle size distribution in the precursor powders. The effect of particle size on ceramics properties can be fairly significant, especially for nanoceramics case. The specifics of this effect in the electrochemical properties can be explained by the changes in the conductivity structure and by the redistribution of the inputs of grain and grain boundary conductivity. So, the information on the particle size both in final ceramics and in precursor powder is very important for the correct treatment of the impedance spectroscopy data, in particular, for the separation of the inputs in the ceramics conductivity.

Table 3 summarizes the data for the particle size in the precursor powders, results of BET estimates, and crystallite size (coherent scattering regions) calculated from XRD data are presented. Note that both approaches are estimates only, nevertheless, it is obvious that one can consider that the particles in the precursor powders manufactured by sol-gel reverse co-precipitation are nanosized objects. However, one should account for the fact that these nanoparicles in the precursor powders are not

Table 2. Ceramic samples composition.

Sample	Composition at synthesis, mol. %			EDX data for final ceramics grain, mol. %		
	ZrO_2	HfO_2	Y_2O_3	ZrO_2	HfO_2	Y_2O_3
1	87	5	8	84.33	6.73	7.18
2	82	10	8	76.86	14.34	7.02
3	77	15	8	72.31	9.90	7.80

Table 3. Estimates for average particle size in the precursor powders according BET theory and calculated from XRD data via Sherrer's formula, nm.

Sample	Estimation from	
	BET	XRD
1	17.8	8
2	18.0	13
3	16.9	12

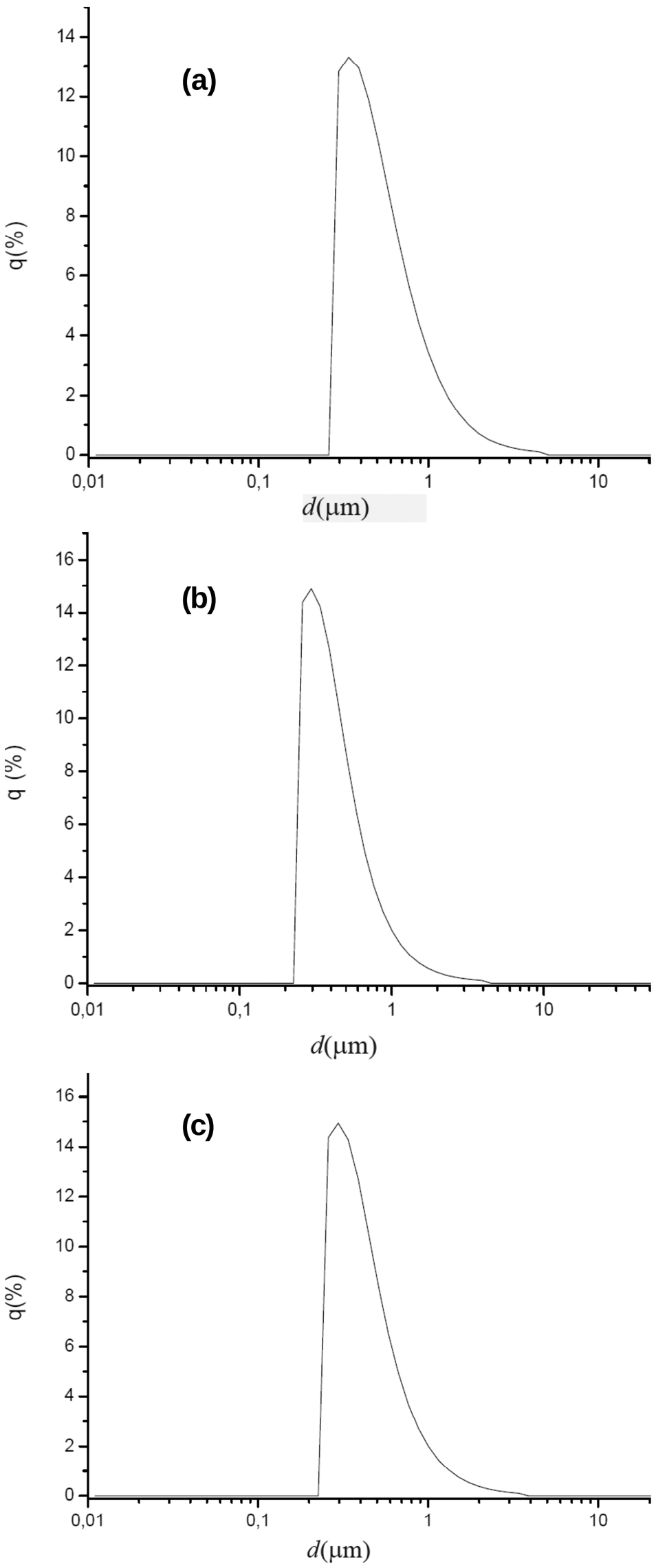

Fig. 2. PSD analysis data for the precursor powders annealed at 600 °C for Sample 1 (a), 2(b), and 3(c).

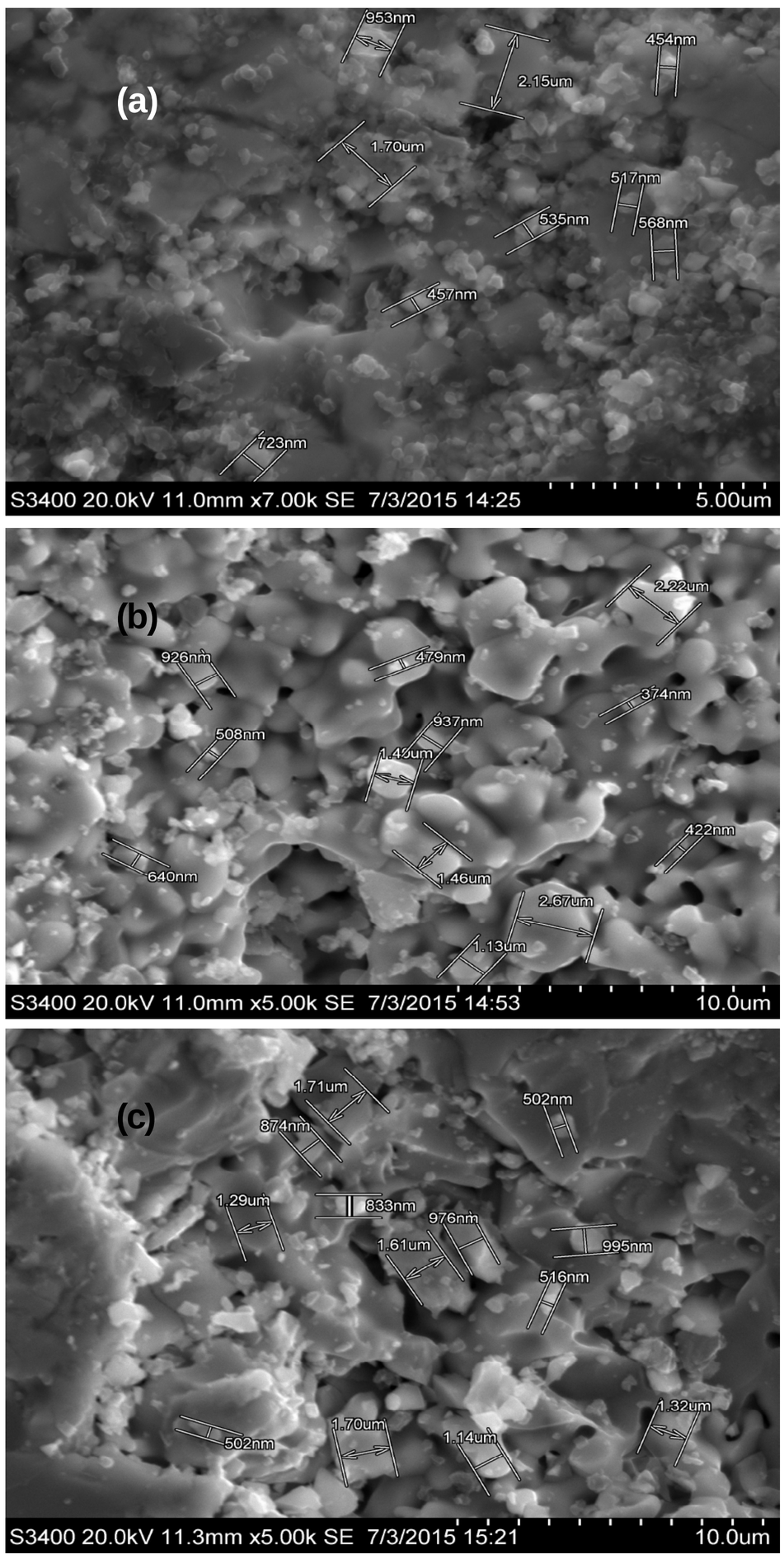

Fig. 3. SEM data for the grain size in Sample 1 (a), 2(b), and 3(c).

stable, the general tendency is their agglomeration. This fact can be proved by the results of PSD analysis, see Fig. 2. It is well known that PSD analysis results (based on laser scattering) characterize particle agglomerates, while absorption-desorption (BET) and XRD data should be attributed to particles themselves. According to PSD analysis data, the average agglomerate size is 568, 465, and 468 nm for samples 1, 2, and 3, respectively. Significant agglomeration also results from powder compacting and annealing, the effect of these synthesis steps on the particle size requires additional investigations. Fig. 3 shows the results of SEM determination of the grain sizes in the final ceramics. The presented data support the above statement on the additional particle agglomeration due to precursor powder compacting and annealing. As

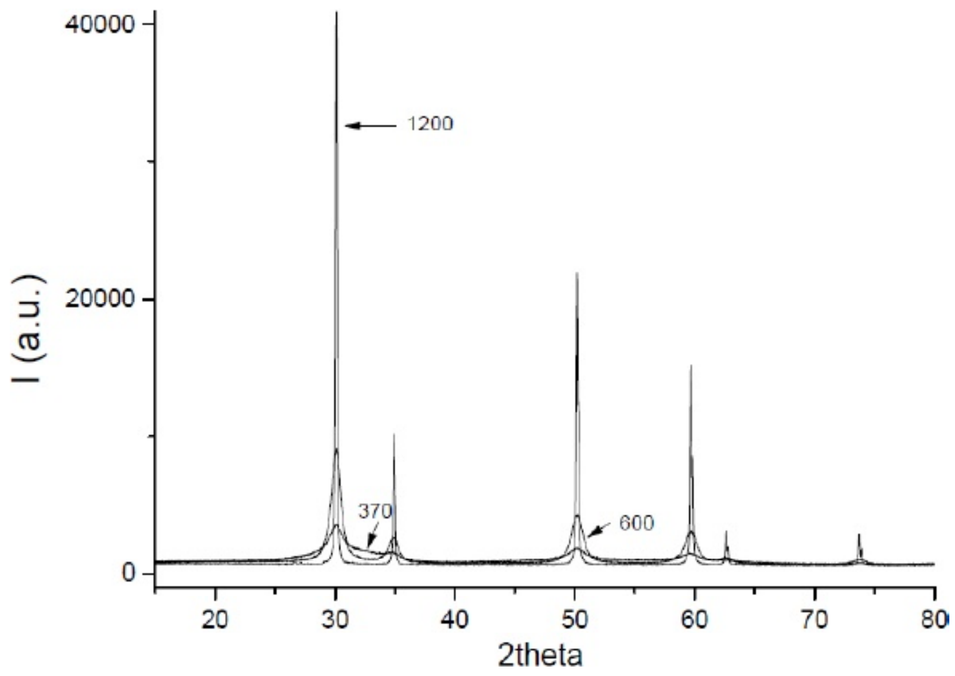

Fig. 4. XRD patterns for Sample 1 powder annealed at different temperatures.

seen from the figure, typical grain sizes in all final ceramics are in the range from 500 nm to 2 μm, these dimensions exceed nanosize range.

Summarizing the above consideration, we can state that chemical composition of the samples does not significantly affect the particle size in the precursor powder and grain size in final ceramics. The increase in the average particle size is due to ceramic formation procedures. Special efforts should be undertaken to minimize the final ceramics grain size down to nanoscale.

3.4. Phase composition

The study of the phase composition was based on the above discussed DSC results. Regarding for effects observed on DSC curve, the precursor powders were annealed at 370, 450, 600, 1000, and 1200 °C and the annealed powders were studied by XRD. Typical XRD patterns are depicted in Fig. 4, data for Sample 1 powder annealed at 370, 600, and 1200 °C are shown to demonstrate the general phase composition changes.

As seen from Fig. 4, the onset of the amorphous powder crystallization is observed at 370 °C, but the structure is not formed yet. XRD patterns support the above discussed onset of crystallization at this low temperature; however, DSC data for Sample 1 powder (see Fig. 1a and Table 1) did not show corresponding exothermic effect in 300-400 °C region. As follows from DSC data, crystallization effect for Sample 1 powder manifests itself at 506 °C, so, one can expect the support for these data from XRD-pattern of the powder annealed at 600 °C. Indeed, the analysis of XRD data indicated the presence of fluorite-like cubic structure here, this structure is also typical for $92ZrO_2$-$8Y_2O_3$ and $92HfO_2$--$8Y_2O_3$ solid solutions [13,14] annealed at similar temperatures. The behavior of solid solution at higher temperatures is very important due to the specifics of the materials exploitation, see, e.g., the discussion of the fuel cell requirements in Section 1. As seen from XRD pattern determined for powder annealed at 1200 °C, phase composition here is the same as for powder annealed at 600 °C (fluorite-like cubic structure), however, the crystallinity level at high temperature increases up to 94%. Mention that this increase in crystallinity level is accompanied by the grain size increase (see Fig. 3).

Samples 2 and 3 showed similar behavior, see Fig. 5 demonstrating XRD patterns for powders annealed at 600 °C. The formation of the same fluorite-like cubic structure is observed for these powders. Since the tendencies of the phase composition transitions at annealing are similar for ternary ZrO_2-HfO_2-Y_2O_3 solid solution samples with relatively low HfO_2 and Y_2O_3 content, one can assume similar electrochemical properties of these samples.

3.5. Electrochemical properties

The approaches for the impedance spectra consideration in case of zirconia-based systems were developed following the basic ideas of impedance

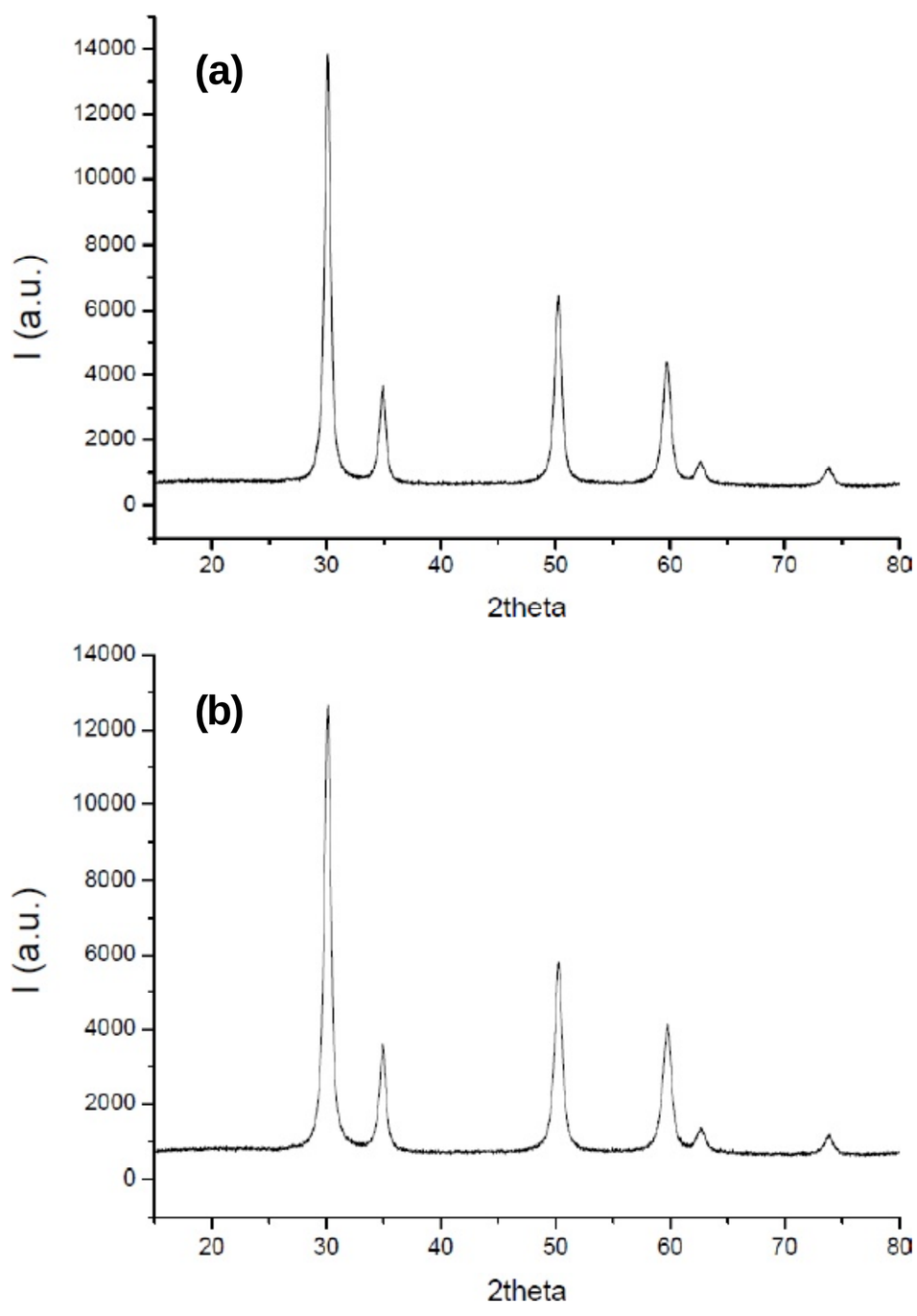

Fig. 5. XRD patterns for powders annealed at 600 °C: Sample 2 (a) and Sample 3 (b).

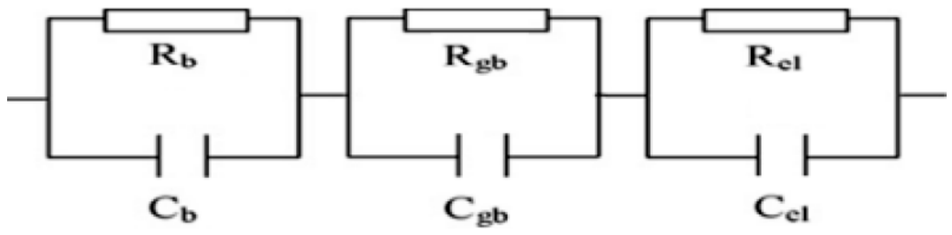

Fig. 6. Equivalent circuit used for the treatment of the impedance spectra of zirconia-based solid solutions.

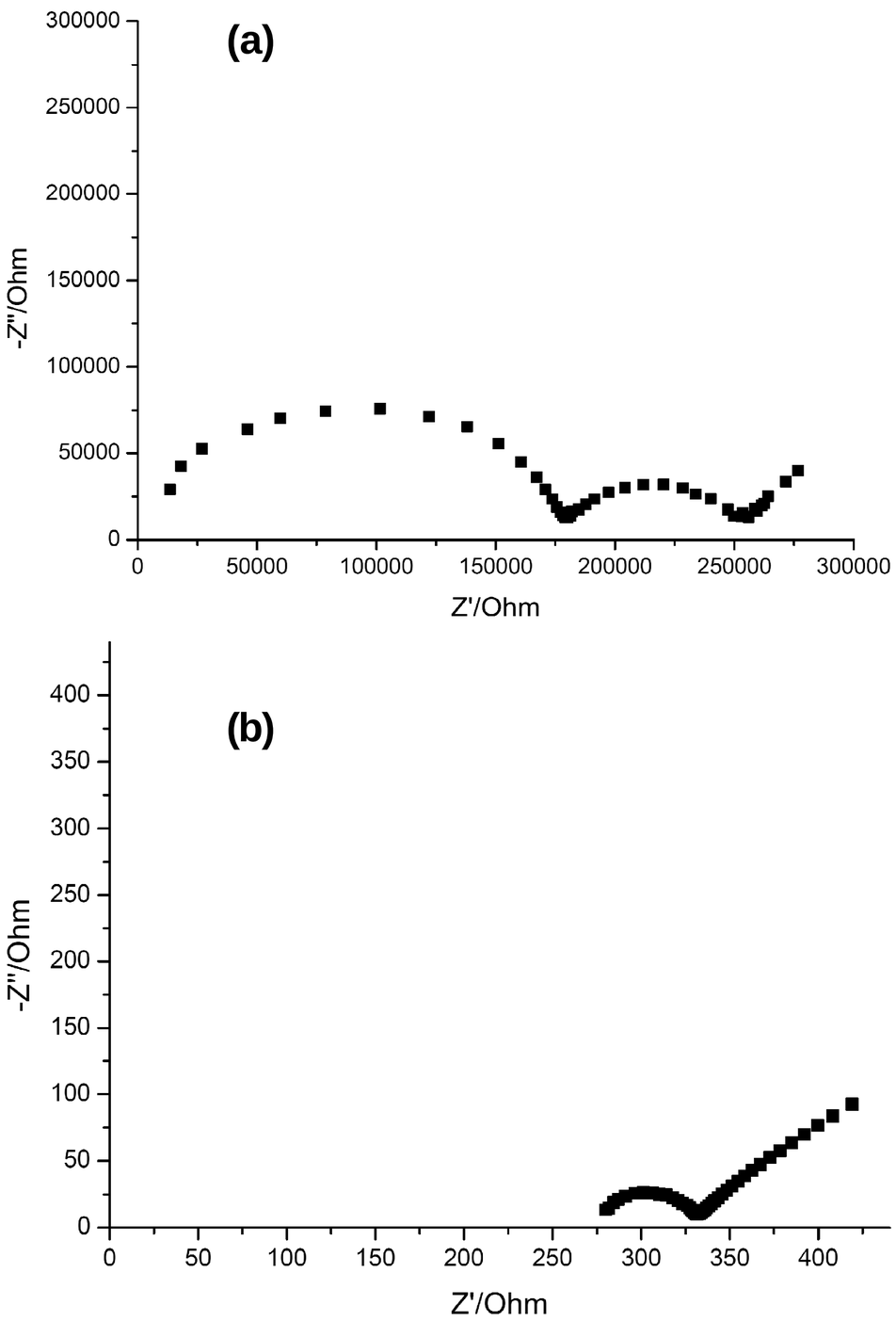

Fig. 7. Impedance spectra taken for Sample 1: (a) at 300 °C, (b) – at 550 °C.

spectroscopy suggested in [15]. Conventionally, three semicircles are considered in the impedance spectrum: high-frequency one corresponding to the grain input in the integral conductivity, mid-range semicircle, corresponding to grain boundary conductivity input, and low-frequency one for the electrode input. At that, the latter semicircle is usually weakly expressed or even indistinguishable. Proper equivalent electrical circuits providing similar impedance spectrum should be chosen to interprete impedance characteristics. Fig. 6 shows the equivalent circuit used for zirconia-based materials consideration. The impedance spectra modeling according to equivalent electric circuits was performed using “Equivcrt” software.

Typical impedance spectra of all samples depend on temperature, two regions should be considered. Conventional three semicircles are observed for all samples studied at temperatures from 250 to 450 °C, see the example of such spectrum in Fig. 7a presenting Sample 1 impedance spectrum at 300 °C. However, the onset of the high-frequency semicircle (corresponding to grain conductivity) degeneration is observed even at that temperature. The following temperature increase up to 450 °C results in complete disappearance of high-frequency semicircle; at higher temperatures it is absent, see, e.g. Fig. 7b – impedance spectrum of Sample 1 at 550 °C. Hence, calculation of the grain resistivity here was carried out using the data on the mid-range semicircle intercept with *Z*’ axis, i.e. its shift from zero point. Similar temperature behavior of the impedance spectra was reported in [16] for ZrO_2-CaO system samples. It should be mentioned that the authors of this work considered some alternative semicircle attribution and unconventional equivalent electric circuit stating that high-frequency semicircle is typical for materials with relatively high grain resistance (R_g) *and* grain boundary or intergrain resistance (R_{gb}) values while high-frequency circle passing through the zero point is due to parallel conductivity pathway.

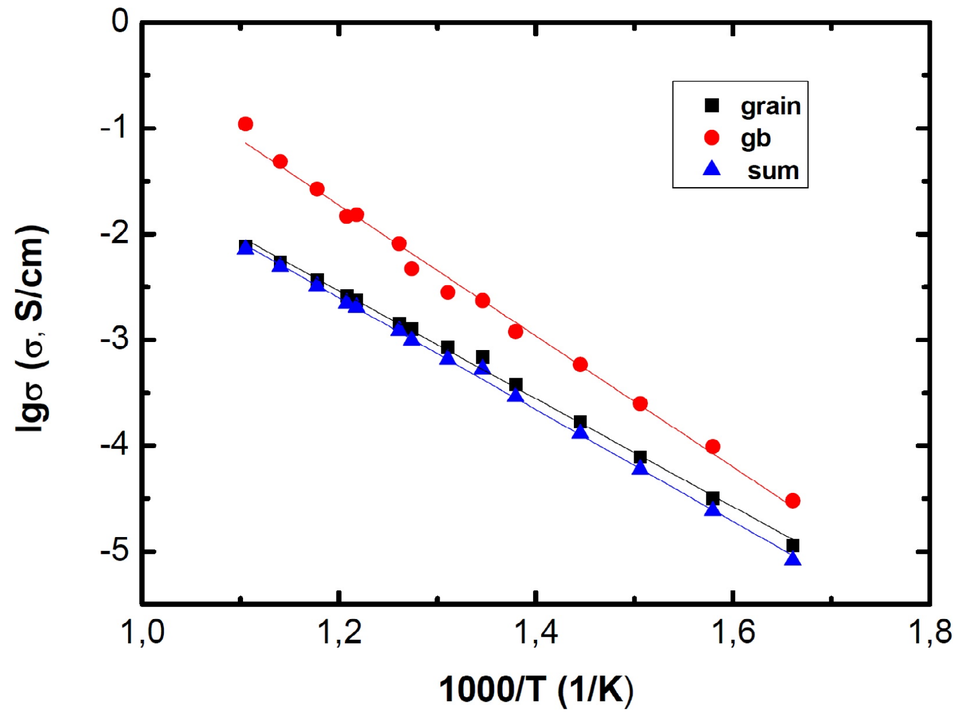

Fig. 8. Arrhenius plots for the different conductivity inputs determined for Sample 1.

Let us consider in some more detail the Arrhenius curves typical for the samples with different chemical composition starting from more simple cases of Samples 1 and 3. The curve obtained for Sample 2 is rather complex and requires specific consideration. Fig. 8 demonstrates the temperature dependencies of grain, grain boundary, and integral conductivities determined for Sample 1, similar behavior shows Sample 3, see Fig. 9. It should be noted that the slopes of grain and grain boundary relative conductivity plots are almost identical for both samples. At that, the values of grain boundary con-

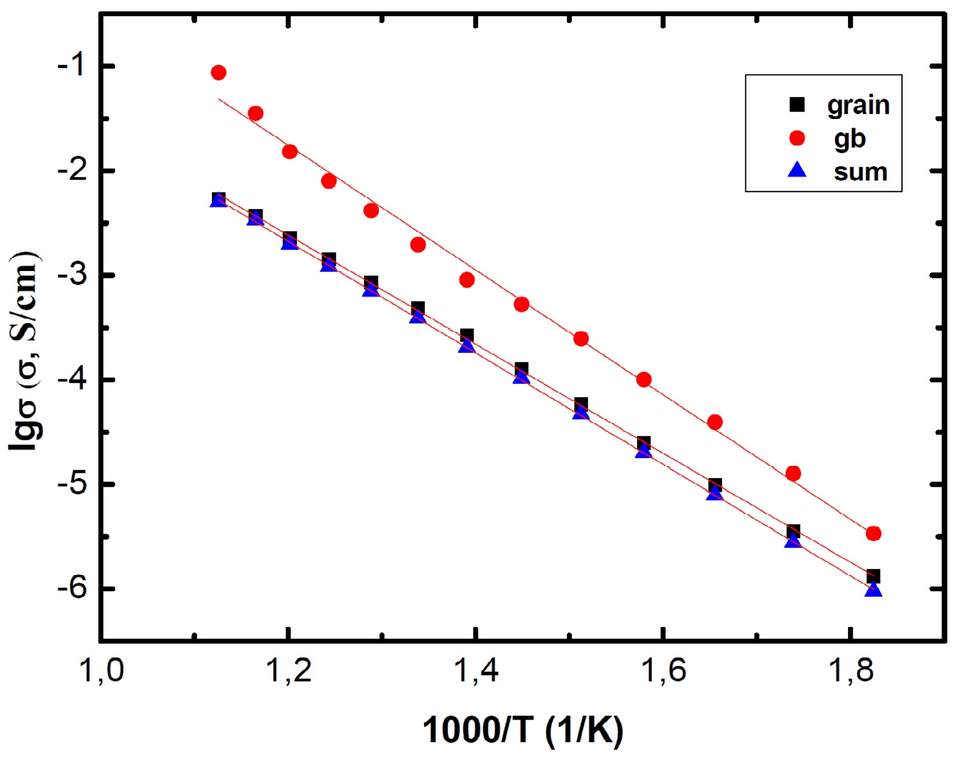

Fig. 9. Arrhenius plots for the different conductivity inputs determined for Sample 3.

ductivity are higher than that for the grain conductivity. Such a behavior is not typical for the ceramics described within conventional Brick Layer Model (BLM). In addition, the semicircle corresponding to grain boundary conductivity on the impedance curves of Samples 1 and 3 is lower that semicircle corresponding to grain conductivity (in case when the latter one is observed). Such a behavior is typical for the discrete grain boundary phase, so, the partially blocking model should be used to consider materials conductivity instead of BLM approach.

Let us now consider the conductivity temperature dependencies for Sample 2. A kind of curve band is evidently seen on the Arrhenius curves of this sample at temperatures ~500 °C, see Fig. 10a. It should be also mentioned that in spite of the identical curve slopes for grain and grain boundary conductivities, the values of these conductivities are quite close. Surprisingly, the repeated impedance study of the same sample carried out after two weeks exposure did not show the curve bend, see Fig. 10b, while the values of grain and grain boundary conductivities are still close. To study the nature of the curve bend, an additional sample with similar composition was synthesized, it demonstrates similar behavior – curve bend at primary impedance study and bend absence in a second one preformed after two weeks exposure. Such a behavior is hard to explain, possibly it is due to specific structure of solid solution with a given chemical composition, this problem requires an additional thorough study.

Basing on the data obtained for Samples 1,2, and 3, the values of the activation energies for the different conductivity types were calculated. The Arrhenius equaion:

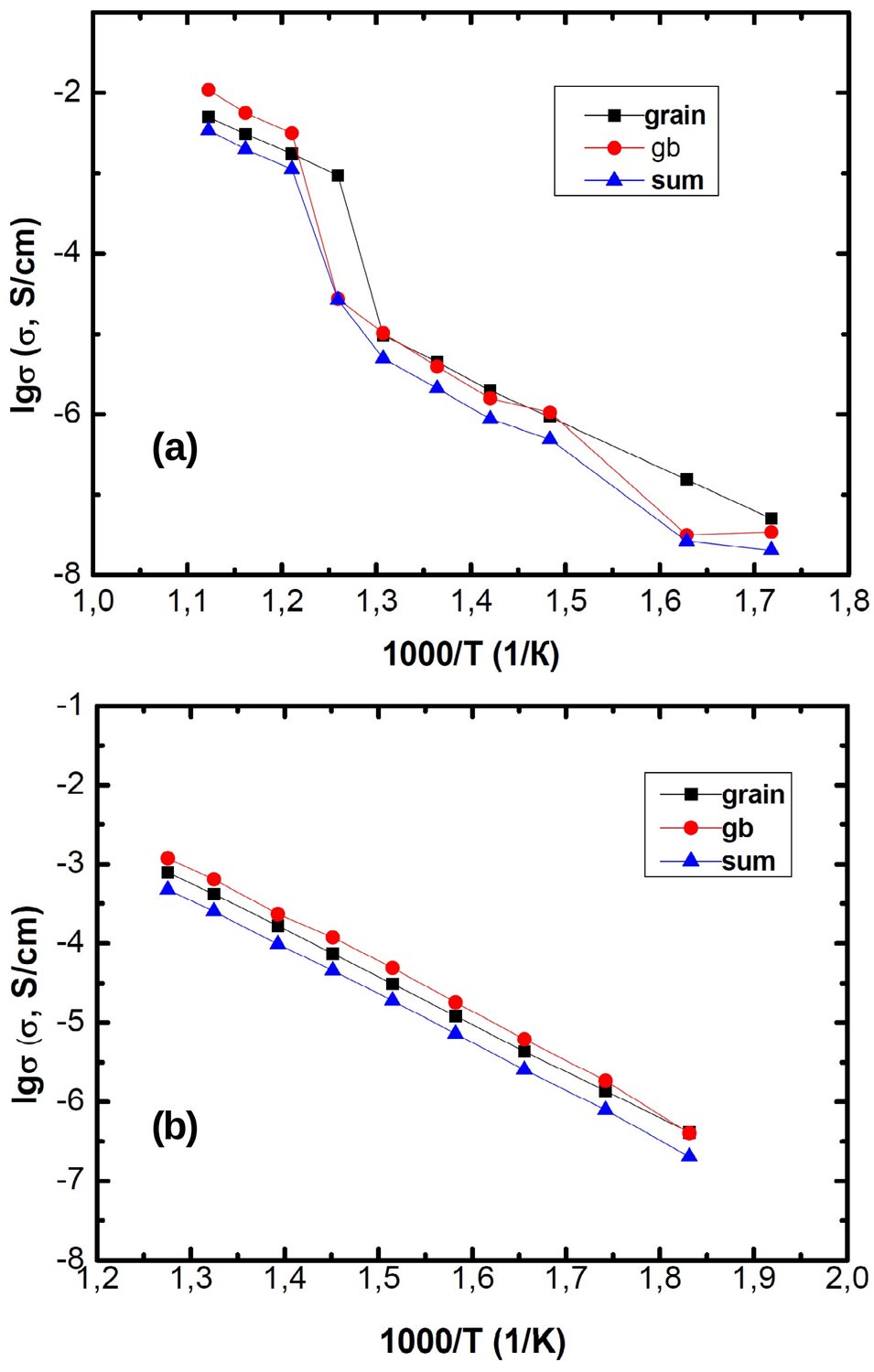

Fig.10. Arrhenius plots for the different conductivity inputs determined for Sample 2: (a) – primary cycle, (b) – secondary cycle.

$$\sigma = \sigma_0 \exp\left(-\frac{E_A}{RT}\right),$$

where E_A is the activation energy, T – absolute temperature, and $\sigma_0 = 0$ at $T \to \infty$, was rewritten with regard to the fact that $\sigma = 1/\rho$:

$$E_A = \frac{2.303R\left(\lg\rho_1 - \lg\rho_2\right)}{\left(\frac{1}{T_1} - \frac{1}{T_2}\right)}, \qquad (3)$$

where ρ_1 and ρ_2 are the resistivities at T_1 and T_2, respectively. Results of the activation energy calculation performed using Eq. (3) are shown in Table 4. Note that data from the second cycle of impedance study (i.e. curves without a bend) were taken to calculate the activation energies for Sample 2; this approach gives an opportunity to compare these data with the results computed for Samples 1 and 3. Summarizing the data presented in Table 4, one can conclude that the activation energy of the grain boundary conductivity is slightly higher than that for

Table 4. Activation energy of the conductivity, kJ/mole.

Conductivity type	Sample 1	2	3
Grain	97.6	105.8	99.8
Grain boundary	118.4	110.3	114.2
Integral	104.7	107.8	102.0

grain conductivity. The dependence of the conductivity activation energy (both for inputs and integral one) on the chemical composition of the material, in particular, hafnium dioxide content, is very weak. At the same time, the comparison of the values determined for hafnium-containing samples with similar values measures for conventional YSZ ceramics ($92ZrO_2$-$8Y_2O_3$ composition, see [17]) indicated that the activation energy for ternary compounds is 1.5 times higher than those for binary YSZ.

Fig. 11 depicts the dependence of the ceramics electroconductivity of HfO_2-containing samples at 760 °C. As seen from the figure, maximal conductivity is observed at 5-6 mol.% HfO_2, it decreases down to local minimum at 15 mol.% HfO_2 with further increase. These data contradict the results for conductivity measurements obtained at constant frequency current [9], possibly it is due to geometric factors.

4. CONCLUSION

Structural features and electric conductivity of the ceramics based on ternary ZrO_2-HfO_2-Y_2O_3 system has been studied. Yttrium oxide content in the studied samples was set as 8 mol.% that is typical for conventional YSZ solid electrolytes used in electrochemical devices, while hafnium dioxide content was varied from 5 to 20 mol.%. It is shown that sol-gel synthesis in the reverse co-precipitation version provides the possibility to produce nanosized precursor powders; their thermal treatment results in the formation of fluorite-like cubic solid solutions. However, the process of final ceramics manufacturing (pressing and annealing at 1500 °C) prevents the synthesis of the material with nanosized grains. Impedance spectra study indicates that such ceramics could not be considered within conventional Block Layer Model, it is reasonable to use Partially Blocking Model here. Maximal conductivity is observed for the ceramics with minimal HfO_2 content.

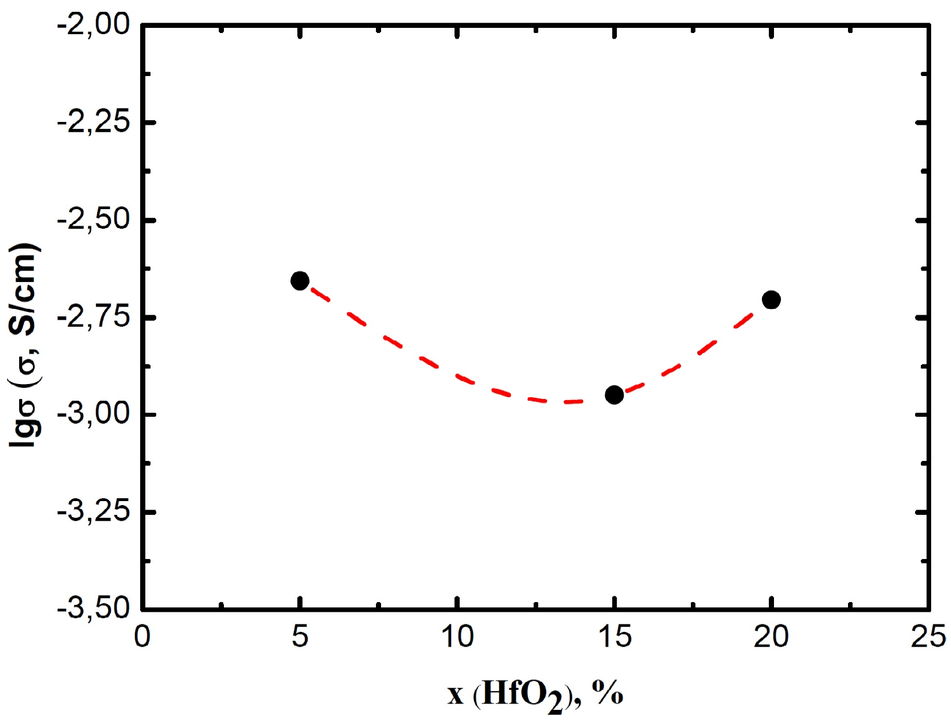

Fig. 11. Ceramics conductivity vs hafnium oxide content in a sample.

ACKNOWLEDGEMENTS

This work was supported by the Russian Science Foundation (Research Project 14-29-00199).

REFERENCE

[1] H.-J. Neef // *Energy* **34** (2009) 327.
[2] N.Q. Minh // *J. Am.Ceram. Soc.* **76** (1995) 563.
[3] M.O. Zacate, L.Minerviny, D.J.Bradfield, R.W.Grimes and K.E. Sickafus // *Solid State Ionics* **128** (2000) 243.
[4] N.N. Novik, V.G. Konakov and I.Yu. Archakov // *Rev. Adv. Mater. Sci.* **40** (2015) 188.
[5] S. Zhuiykov // *J.Europ.Ceram.Soc*. **20** (2000) 967.
[6] M. de Ridder, R.G. van Welzenis, A.W.Denier van der Gon, H.H. Brongersma, S. Wulff, W.-F. Chu and W. Weppner// *J. Appl. Phys*. **92** (2002) 3056.
[7] R.K. Slotwinsky, N. Bonanos and E.P.Butler // *J. Mater. Sci.* **4** (1985) 641.
[8] T.I. Panova, V.B. Glushkova, A.V. Lapshin and V.P. Popov // *Glass physics and chemistry* **29** (2003) 93.
[9] Impedance Spectroscopy: Theory, Experiment and Application, ed. by E. Barsoukov and J.R. Macdonald (Willey, 2005).
[10] O.Yu. Kurapova and V.G. Konakov // *Rev. Adv. Mater. Sci.* **36** (2014) 177.

[11] O.Yu. Kurapova, V.G. Konakov, S.N. Golubev, V.M. Ushakov and I.Yu. Archakov // *Rev. Adv. Mater. Sci.* **32** (2012) 112.
[12] H.L. Tuller // *Solid State Ionics* **131** (2000) 143.
[13] V.S. Stubican, R.C. Hink and S.P.Ray // *J. Am. Ceram. Soc.* **61** (1978) 17.
[14] C. Wang, M. Zinkevich and F. Aldinger // *J. Amer.Ceram. Soc* **89** (2006) 3751.
[15] J.E. Bauerle // *J. Phys. Chem. Solids* **30** (1969) 2657.
[16] S.H. Chu and M.A. Seitz // *J. Solid State Chem.* **23** (1978) 297.
[17] N.V. Korovin, *Fuel Cells and Electrochemical Power Plants* (Moscow, MAI, 2005), In Russian.